Journal of Alloys and Compounds 523 (2012) 1–10

Contents lists available at SciVerse ScienceDirect

Journal of Alloys and Compounds

journal homepage: www.elsevier.com/locate/jallcom

Peculiarities of the neck growth process during initial stage of spark-plasma, microwave and conventional sintering of WC spheres

Dmytro Demirskyi[a,b,*], Hanna Borodianska[b,c,d,1], Dinesh Agrawal[a,2], Andrey Ragulya[b,1], Yoshio Sakka[c,3], Oleg Vasylkiv[c,d,4]

[a] Materials Research Institute, The Pennsylvania State University, University Park, PA 10802, USA
[b] Frantsevich Institute for Problems in Material Science, 3 Krzhizhanovsky Str., 03680 Kyiv-142, Ukraine
[c] National Institute for Materials Science, 1-2-1 Sengen, Tsukuba-city, Ibaraki 305-0047, Japan
[d] Nanyang Technological University, 50 Nanyang Avenue, 639798 Singapore, Singapore

ARTICLE INFO

Article history:
Received 24 October 2011
Received in revised form 25 January 2012
Accepted 27 January 2012
Available online 8 February 2012

Keywords:
Microwave heating
SPS
Sintering
Diffusion mechanism
Ceramics

ABSTRACT

This work involves an investigation of the neck growth kinetics of free-packed spherical shaped binderless tungsten carbide particles during microwave and spark-plasma sintering. The application of a classical sphere to sphere approach showed the possibility of identifying the main diffusion mechanisms operating during the initial stage of microwave sintering of tungsten carbide powder. An anomalous neck growth rate in the initial period during microwave and spark-plasma sintering processes, up to 100 times faster in comparison to conventional sintering, was also revealed. Volume diffusion was enhanced by a small amount of a liquid phase, and surface diffusion was proposed as the primary mass transport mechanism for microwave sintering. The simulation operation of grain-boundary diffusion and power law creep was responsible for neck growth during spark-plasma sintering.

Numerical simulation of neck growth revealed high values of the diffusion coefficient for microwave (3.41×10^{-8} m^2 s^{-1} at 1200 °C) and spark-plasma sintering (5.41×10^{-8} m^2 s^{-1} at 1200 °C). In the case of conventional sintering, the diffusion coefficients calculated are in good agreement with values for diffusion of W and C in a W–C system (8.6×10^{-16} m^2 s^{-1} at 1200 °C).

Low values of the apparent activation energy (E_a) for microwave and spark-plasma sintering (62 and 52 kJ mol^{-1}) have been obtained. For conventional sintering, all data collected indicate grain-boundary diffusion as the primary sintering mechanism (272 kJ mol^{-1}).

1. Introduction

For almost decade the SPS technique has been successfully applied to consolidate the various metals, alloys, ceramics, its composites [1–6] providing rapid heating and high densification rates at lower processing temperatures, accompanied by a very limited grain growth [7]. The majority of investigations applying the SPS consolidation technique have focused on obtaining bulk materials with desired microstructure and properties. In contrast, just a few studies been focused on the underlying the fundamental aspects and phenomena of the SPS process itself [8,9]. The application of an electric current for direct heating of the conductive samples contributes to one of the characteristics of the process: high heating rates. Heating rates of up to about 2000 °C min^{-1} can be achieved by applying SPS method [1]. In addition, the role of the pulsed current, other than that of providing Joule heating, has been widely associated with creating a plasma which activates the surface of powder particles. Such activation is reported, for example, to remove impurity surface layers (e.g., oxides) [10]. However, the existence of a plasma has not been unambiguously proved, even the several reports bring forth contradictory findings [11,12].

In addition, the role of the current as a non-thermal parameter (i.e., other than Joule heating) has been considered in only a few investigations. Several previously proposed theories [13,14] were mainly focused on the intermediate and final stage sintering. It was clarified that grain-growth and densification kinetics are not governed by classical sintering mechanisms [15]. These phenomena are usually explained by accompanying the spark-plasma

* Corresponding author at: Frantsevich Institute for Problems in Material Science, 3 Krzhizhanovsky Str., 03680 Kyiv-142, Ukraine. Tel.: +380 44 424 7435; fax: +380 44 424 2131.
E-mail addresses: dmytro.demirskyi@gmail.com, dxd43@ipms.kiev.ua (D. Demirskyi), borodianska@ipms.kiev.ua (H. Borodianska), dxa4@psu.edu (D. Agrawal), ragulya@ipms.kiev.ua (A. Ragulya), sakka.yoshio@nims.go.jp (Y. Sakka), oleg.vasylkiv@nims.go.jp (O. Vasylkiv).
[1] Tel.: +380 44 424 7435; fax: +380 44 424 2131.
[2] Address: 107 MRL Bldg., Penn State University, University Park, PA 16802, United States. Tel.: +1 814 863 8034; fax: +1 814 865 2326.
[3] Tel.: +81 029 859 2461.
[4] Tel.: +81 029 859 2673.

0925-8388/$ – see front matter © 2012 Elsevier B.V. All rights reserved.
doi:10.1016/j.jallcom.2012.01.146

sintering with electromigration process during processing of conductive materials [16,17]. In contrast the pressure-driven mechanisms of creep and dislocation movement are usually considered for densification of insulating oxides. Alternatively it is thought that high heating rates [15] and local temperature gradients [18–21] generated inside the 'body' of each powder particle, which is mainly a porous aggregate with non-homogeneous morphology, are responsible for acceleration of the local densification processes.

Model experiments on SPS by a sphere-plate model also revealed enhanced neck growth under the influence of electrical current. Such enhancement was attributed to electromigration [16,22]. Yet the effect of electric current or electric field is not clearly addressed. Recent work of Cologna and Raj [23] revealed the surface diffusion driven densification during initial stage consolidation of YSZ ceramic by electric field sintering. However the same activation energy of the densification process was found in the presence of the electric field or without it [23].

Surprisingly on the stage of neck formation of bulk zirconia spheres the similarities in microstructure have been found while comparing the SPS and microwave sintering (MWS) [21]. As for later, recent works on the initial stage sintering of pure metals [24–26] and WC [27] suggested that non-conventional sintering mechanism may operate during initial stage of microwave sintering. The anomalous neck growth rates were also revealed, suggesting increase in diffusivity during sintering process. Since both processes (SPS and MWS) provide high-heating rates [1,28] the possible comparison between two processes is intriguingly attractive.

Therefore, in order to understand the neck growth stage during the SPS, for present paper we proposed a classical sphere to sphere model [29,30] of studying the initial stage of sintering during consolidation of spherically shaped tungsten carbide powder. The sufficient database for comparative study been previously obtained from microwave [27] and conventional sintering (CS) of the same powder. The second aim of the current study is to propose and clarify the mechanisms controlling the initial stage of spark-plasma sintering and its comparing with microwave and conventional sintering.

2. Materials and methods

In this study, superhard fused spherical tungsten carbide powder was used (Rilit™, manufactured by Paton Electric Welding Institute, Kyiv, Ukraine). Particle size distribution (SEM, MasterSizer 2000, Malvern) and phase/chemical analysis by XRD/EDX techniques were determined to characterize the initial powder.

A series of classical neck growth kinetics experiments was conducted using the sphere-to-sphere approach [24,29,30], in order to investigate the diffusion mechanisms that control the initial stage of SPS, microwave and conventional sintering of binderless WC powder.

2.1. Temperature measurements

In case of MWS the temperature was monitored using infrared pyrometer, Raytek MA2SC (working temperature range 350–2000 °C), from samples' surface and recorded in situ by a computer, at the temperatures higher than 800 °C second pyrometer (Minolta/Land Cyclops 152, Land Infrared, Bristol, PA) was used for reference. Both pyrometers were calibrated using melting temperatures of copper, silver and nickel (an error of ±6 °C was assumed to be satisfactorily for MWS experiments).

In case of SPS the temperature was monitored by two pyrometers: from the top and from the side of the graphite die. The possible temperature gradients during SPS processing of WC using this set-up is provided elsewhere [31], we used the same approach to evaluate temperature in the present work.

2.2. Spark-plasma sintering

The spark-plasma sintering experiments (SPS) were performed in an SPS apparatus (Dr. Sinter Model 1050, Sumitomo Coal Mining Co. Ltd., Japan) in nitrogen gas. The tungsten carbide particles were loaded in a graphite die (10 mm in diameter) and punch unit. Graphite foils (Grafoil) were used as spacers between the specimen and the graphite die and punches. In a typical experiment, 0.8 g of the powder was loaded into the die, without preliminary pressing, which was then placed inside the SPS apparatus [4]. A low pressure of 25 MPa (2.0 kN) was initially applied. Each specimen was first heated to 600 °C, exposed for 1 min, and then heated to the preset temperature (900, 1200 and 1400 °C) at heating rates of 150 °C min^{-1} at a starting current of 400 A. The temperature was measured using a pyrometer. The specimen was gradually cooled down to 600 °C at a cooling rate of 20 °C min^{-1} and then furnace-cooled to room temperature.

2.3. Microwave sintering

We used a 6 kW multimode microwave applicator 2.45 GHz in the present study, the in-depth information upon experimental set-up is presented elsewhere [27,32]. An inert atmosphere was maintained during the sintering process by first creating a vacuum of 8–10 Torr inside the furnace by back filling ultra high purity (UHP) nitrogen. Throughout the sintering, nitrogen gas flow was maintained at 2 L min^{-1}. A heating rate of 150 °C min^{-1} was maintained during the heating process to soaking temperature by adjusting the microwave applicators' power level. After the sintering temperature was reached, isothermal holding was applied. After sintering, the microwave power was switched off and the samples were allowed to cool in the furnace (typical cooling rate was 15–30 °C min^{-1}).

2.4. Conventional sintering

The conventional sintering experiments were carried out using a tube furnace (max. temp. 1600 °C) in nitrogen gas with a flow rate of 2 L min^{-1}. Prior to sintering, the tungsten carbide powder was covered with graphite foils (Grafoil) and placed into the graphite crucible. A heating rate of 10 °C min^{-1} was used to reach soaking temperature; after isothermal soaking for a specific period, the samples were allowed to furnace-cool with cooling rate of 20 °C min^{-1}.

2.5. Characterization

After sintering, a batch of sintered spheres was examined by SEM (JSM-7001F, Hitachi S-3500N) to investigate the neck size and structure. A monolayer of sintered spheres was divided into parts in order to investigate the neck zone structure and neck size. A group of spheres were then placed on a copper foil in order to eliminate the influence of the carbon foil during phase analysis. The phase composition of the sintered samples was determined by nano-area energy-dispersive X-ray spectroscopy (EDX), and by XRD analysis using a RINT 2000 X-ray diffractometer (Rigaku, Tokyo, Japan) with Cu Kα radiation at 40 kV and 50 mA at room temperature.

2.6. Neck growth kinetics—a sphere-to-sphere approach

Sintering normally occurs in three sequential stages referred to as the initial stage, the intermediate stage, and the final stage. The initial stage of sintering generally consists [33] of fairly rapid interparticle neck growth by diffusion, vapor transport, plastic flow, or viscous flow. The large initial differences in surface curvature are removed in the first stage, and shrinkage (or densification) accompanies neck growth for the densification mechanisms. The neck formed between the particles is assumed to be circular with a radius x and with a particle radius to be marked as a.

Thus the derivation of the initial stage sintering equations can be presented [29,30] as

$$(x/a)^n \sim B \cdot t \quad (1)$$

where x/a is the ratio of the interparticle neck radius to the particles radius, B is a constant (includes particle size, temperature and geometric and materials terms), t is sintering time, and n is the mechanism-characteristic exponent which is dependent on the mass transport process.

It should be noted that originally initial stage sintering experiments were also used as an indirect method of obtaining diffusion coefficients [34,35], with rate constant $B = B_0 \exp(-Q/RT)$, and B_0 includes a diffusion coefficient (Table 1) [36], and apparent activation energies of diffusion processes (Q_a). These values are also derived from the neck growth kinetics and may be used to verify the values of n if required.

During the current investigation the particles were examined for neck size, particle size and change in interparticle distance. In order to ensure validity of the measured data [37], the number of necks measured for every point exceeded 15, the average data for neck size was used as x, $x = 1/z\sum_{i=1}^{z} x_i$, where x_i is the neck size in μm, and z is the number of measurements of the neck under the given sintering conditions, $z \geq 15$. Relevant standard deviations from the mean neck size were used during preparation of the neck growth kinetics plots.

3. Results and discussion

3.1. Characterization of powder

The particle size distribution of tungsten carbide powder revealed that the mean particle size is 127.7 ± 5.2 μm with a

Table 1
Values of sintering rate exponent n and pre-exponent kinetic parameter B_0 for main diffusion mechanisms (after German [36]).

Sintering mechanism	n	m	B_0 ($m^m\ s^{-1}$)
Viscous flow	2	1	$3\gamma/2\eta$
Plastic flow	2	1	$9\pi(\gamma D_v/b^2)(\Omega/RT)$
Evaporation–condensation	3	2	$(\pi/2)^{1/2}(3P\gamma/\rho_T^2)(M/RT)\rho^{3/2}$
Lattice (volume) diffusion	5	3	$80D_v\gamma\Omega/RT$
Grain-boundary diffusion	6	4	$20\delta D_b\gamma\Omega/RT$
Surface diffusion	7	4	$56\delta D_s\gamma\Omega/RT$

B_0 – pre-exponent kinetic parameter, m^m/s; D_b – grain-boundary diffusivity ($m^2\ s^{-1}$); D_s – surface diffusivity ($m^2\ s^{-1}$); D_v – volume diffusivity ($m^2\ s^{-1}$); M – molecular weight (kg/mol); P – vapor pressure (Pa); R – universal gas constant, 8.31 J/(mol K); T – absolute temperature (K); b – Burger's vector (m), m – Herring scaling-law exponent; n – neck-growth exponent; Ω – molar (atomic) volume (m^3/mol); γ– solid–vapor surface energy (J/m^2); δ – diffusion-layer width or thickness (m); η– viscosity (Pa s); ρ_T – theoretical density (kg/m^3).

monomodal PSD curve. SEM measurements of the particle size showed a mean value of 120.2 ± 7.4 μm and the particle shape to be spherical. EDX confirmed W and C as the major elements present, with oxygen at about 1.09 wt% [27]. Oxygen is more likely to be present as free oxygen adsorbed on the particle surface because no oxide phases have been found using XRD.

Moreover, for the initial powder, some traces of a W_2C phase were revealed, caused by the powder production method. For samples sintered via conventional and spark-plasma sintering methods WC was found as the major phase. While for microwave sintering, WC remains as the major phase with a minor phase of W_2C, which was present in the initial powder itself, and the formation of carbon-free tungsten was also revealed. The in-depth explanation of this phenomenon is provided elsewhere [27].

3.2. Neck growth kinetics

Data from SEM investigation of a monolayer of sintered WC particles sintered at different temperatures and soaking times were obtained and the results are shown in Figs. 1 and 2. It should be noted that, for conventional and spark-plasma sintering, neck growth was not observed at temperatures lower than for 800 °C and 1200 °C in the case of SPS and CS, respectively. As for MWS, it was found that the neck formation process starts between 700 and 750 °C. However, for this temperature range, the interparticle necks are few in number, and their size is at the same level with that formed in the 800–950 °C region. Almost all particles in the system have at least two partners at 1000 °C in the microwave sintering case. The deviation from the mean values of (x/a) ratio observed during neck growth measurements is of the order of 9–12%. Such

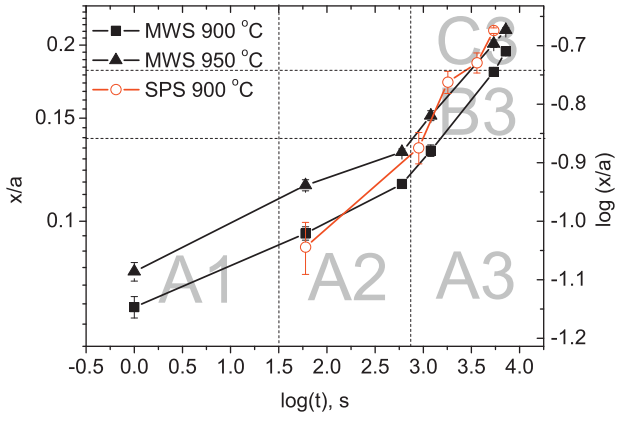

Fig. 1. Neck growth kinetics during microwave and spark-plasma sintering in the temperature region of 900–950 °C.

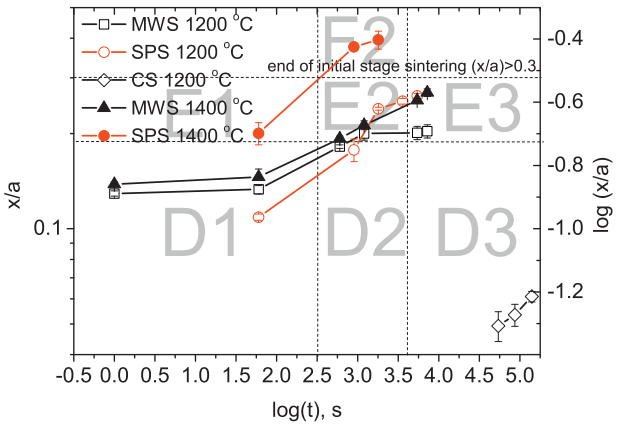

Fig. 2. Neck growth kinetics during microwave, conventional and spark-plasma sintering in the temperature region of 1200–1400 °C.

magnitudes are due to (a) the distribution in sphere sizes, (b) the non-circular shape of some necks and (c) normal statistical variations. Wilson and Shewmon [37] pointed out that a 20% variation in x/a values is to be expected for a given set of sintering conditions and spheres of identical diameter.

In order to verify the structure of the interparticle necks, Figs. 1 and 2 were divided into zones, representing the typical microstructure for given temperature and soaking time. Subsequent data on microstructure for all sintering methods used is presented in Figs. 3 and 4.

Analysis of the experimental data on isothermal neck growth kinetics [33] established that the exponent in $(x/a)^n \sim B{\cdot}t$ relations (Figs. 3 and 4) is in agreement with the volume, surface and grain-boundary diffusion mechanisms.

3.2.1. Spark-plasma sintering

For temperatures of 900–950 °C for SPS, the exponent value of 5.05 was obtained, which is in good agreement with the value that is usually reported in the literature for volume diffusion ($n = 5$) [38]. In the case of SPS, the slope for linear shrinkage for all temperatures observed was in the range of 0.29–0.34, which is in good agreement with the slope that is usually predicted for grain-boundary diffusion (~1/3) [39,40]. This might be an indication that, in the case of SPS, at least two sintering mechanisms are working simultaneously. Importantly, in the case of SPS of metals like aluminum, the simultaneous densification by power-law creep and grain-boundary diffusion was previously observed [17]. Some reports [41] indicate that the contribution of power-law creep is minor (negligible) in the case of the SPS of oxides. Anyhow, the power-law creep in combination with grain-boundary diffusion mechanism might produce a combined neck growth exponent of ~5; therefore, the defined contribution of a single mechanism involved may be considered to be a task for further research.

With an increase in temperature up to 1200 and 1400 °C, exponent values of 4.7 and 4.8 are deduced for 1200 and 1400 °C, respectively. Accompanied by a linear shrinkage exponent was found to be 0.31, like that in the case of lower temperatures applied.

The rise in temperature to 1400 °C significantly affects neck size as well as the structure of the necks (Fig. 4) and overcomes initial stage sintering. The value of $n = 4.8$ was found before the $(x/a) < 0.3$ mark, which is in good agreement with a combination of grain-boundary diffusion and sintering under low pressures applied (or power-law creep). Interestingly, with an increase in soaking times, the neck geometry changes radically and some saturation stage was also found with an inverse slope value of $n = 13$. Further increase in soaking time might result in passing the intermediate sintering

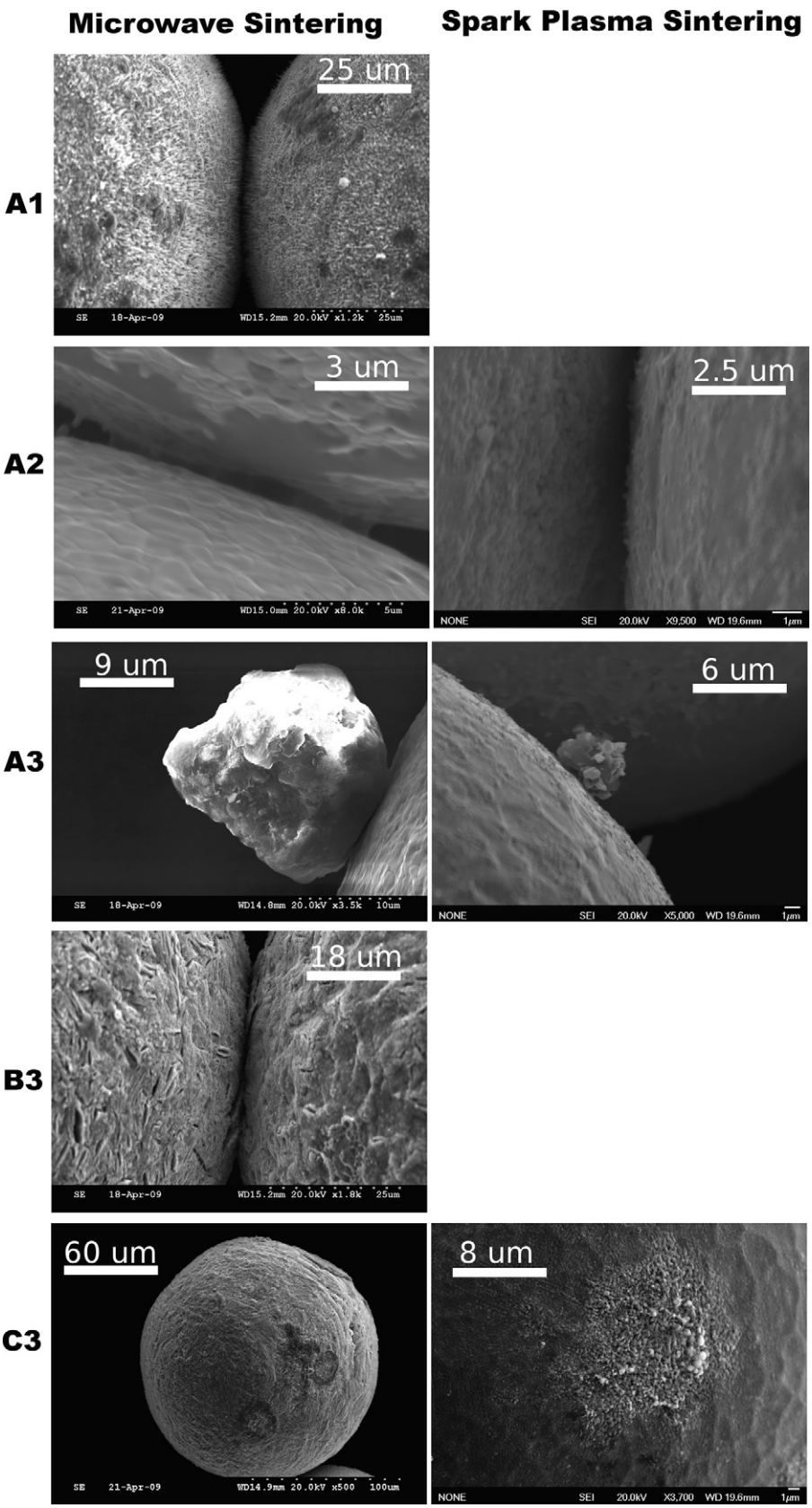

Fig. 3. Structure of neck surface formed during microwave and spark-plasma sintering in the temperature region of 900–950 °C.

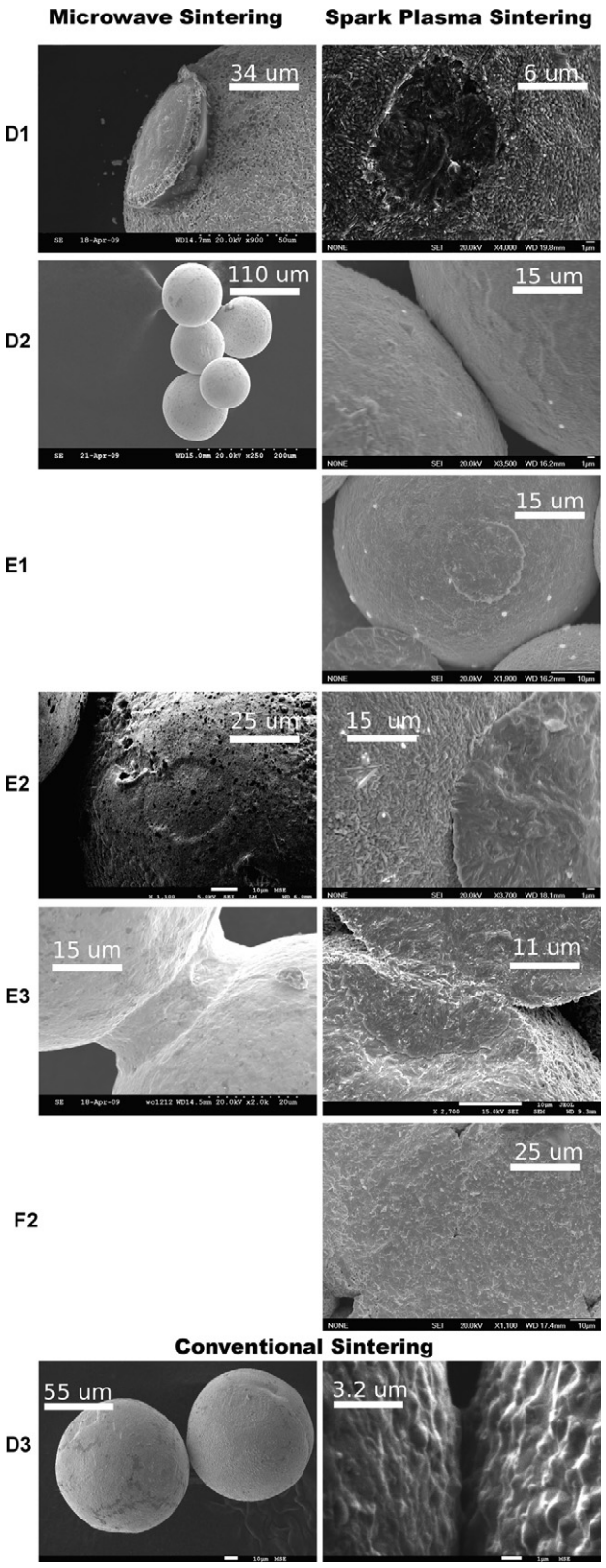

Fig. 4. Structure of neck surface formed during microwave, conventional and spark-plasma sintering in the temperature region of 1200–1400 °C.

stage, as microstructural analysis suggests (Fig. 4 (F2)), but this is not a subject of current research.

3.2.2. Microwave sintering

Division of the neck growth process for microwave sintering into two stages is quite apparent (Fig. 1): with the neck formation process taking place during (i) the heating process at set temperatures and (ii) ending at short soaking times. This division is clearer when comparing lower to higher temperatures, as for the latter (Fig. 2) initial stage, which includes neck formation, and is shorter. This occurs due to additional exposure to microwave energy during ramping up to higher temperatures. While the total value of absorbed energy at the start of the soaking period is almost the same as that for a short period (up to 5 min) of soaking at lower temperatures. The n values of ~80 and are not subject to the conventional neck growth theory [33,35]. An anomalous high value of n has been observed previously for metals [42] and is attributed to the occurrence of simultaneous mechanisms of mass transport with a competing mechanism blocking a shrinkage-producing mechanism. In contrast, the data for conventional and spark-plasma sintering strictly obey the power law with given deviations taken into account.

After this stage is completed for low- and high-temperature region Figs. 1 and 2, respectively, it was found that further neck growth corresponds to volume and surface diffusion, respectively. In confirmation of the former a decrease in the center–center distance of the spheres was observed, indicating that mechanism that induces shrinkage must have taken place. The relationship observed corresponds to $\Delta L/L_0 \sim t^{2/5}$ time dependence that was previously reported for the conventional sintering of copper by volume diffusion [30] and for microwave sintering of copper [25].

Noticeably, for 1200 °C there is a saturation region, so the neck growth kinetics curve looks like a typical S-type curve for densification kinetics during the sintering process [43]. This region with almost no growth in neck length (with $n = 20$) may be explained by exhaustion of the initial driving force (curvature) and that the further growth is impossible unless sintering conditions are changed.

3.2.3. Conventional sintering

As mentioned above, the neck growth process during conventional sintering did not start lower than 1200 °C. Resulting neck growth plot for 1200 °C is presented in Fig. 2 and an exponent of 5.9 was found, suggesting grain-boundary diffusion as the main sintering mechanism. No decrease in center–center distance between spheres was observed for conventional sintering. With the rise in temperature to 1400 °C, there is no significant change in value of neck size for conventional sintering (not shown) with n value of 6.0.

In comparison, data for conventional sintering not only differs from that for MWS and SPS by neck size value, but the neck growth rate is more than 100 times slower (Fig. 5).

Neck formation was not observed until soaking times exceeded 15 h, which is in good agreement with the neck growth rate for grain-boundary diffusion (dashed line) calculated for using the Ashby's approach [38,44,45]:

$$\dot{x} = \frac{4D_b\delta\gamma\Omega/RT}{x}K^2 \quad (2)$$

where $K = (1/\rho - 1/x)$ and $\rho = [x^2/2\ (a-x)]$, Values of a, δ, Ω and γ are taken from elsewhere (Table 2) [46], $x/a = 0.1$, diffusivities for low-temperature region are taken in [47].

3.3. Structures of "necks"

Although the size of the necks as well as the rate exponent seems to be the same for SPS and MWS of WC powder, the structure

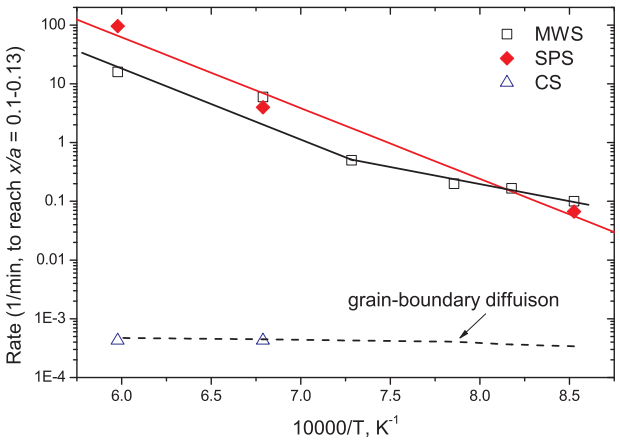

Fig. 5. Temperature dependence of the rate of neck growth between WC spheres. Dashed line represents neck growth rate for grain-boundary diffusion according to Eq. (2) [45].

analysis confirmed that the processes behind the neck growth may have the same kinetics but have different driving forces.

For temperatures of 900–950 °C, the actual neck growth starts with the creation of small sized necks (Fig. 3 (A1–A2)). The surface of particles near the contact areas is clearly covered with small grains (Fig. 3 (A1) – MWS) and (Fig. 3 (A2) – SPS), and the initial grain-size for polycrystalline WC-spheres was ~10 μm. With an increase in processing time, full-sized grains are formed on the particle surfaces (Fig. 3 (A2) – MWS). The interesting point is that a crack in the contacts between the particles seems to occur under the same mechanism (Fig. 3 (A3)) and the surface of the near neck zone appears to be identical. However, with a further increase in processing time (Fig. 3 (B3–C3)), the structure of both the particle surfaces and neck zone areas become radically different. In the case of MWS, some evidence of crystalline structure appears on the particle surfaces, but in the case of SPS, there are small-sized grains in the neck region, while the particle surfaces remain almost the same (Fig. 3 (A3 and B3)). Only for the (C3 – SPS) region in the case of SPS, the grains in the neck region grow and are identical to those for the near-neck area.

With an increase in processing temperatures, few phenomena were observed (Fig. 4): in the case of MWS, there is apparent evidence of either melting and/or a crystal growth process in the neck zone (D1 – MWS), which may be due to the reasons described earlier. What is more important, this feature is being monitored only in the neck region where the particle surface structure for both MWS and SPS is identical (D1). It should also be mentioned that neck structure in the case of SPS appears as large-scaled grains, while the same phase has been found in both cases by EDX (not shown). With an increase in temperature (E1), the same situation is observed, except that the effective neck size is much bigger for SPS 1400 °C than that in the case of MWS.

A further increase in processing time (Fig. 4 (D2 and E2)) leads to an extension of the neck size and "grain" size observed in the neck region, with only one difference, in the case of MWS (E2 – MWS) the formation of a regular-sized grain structure is observed in both the neck area and on the particles' surface. This difference becomes clearer with a further increase in processing time (Fig. 4 (E3) for SPS and MWS): as in the case of MWS, a smooth surface is observed on both the neck and particles' surface, while in the case of SPS, the structure has crystalline, sharp-edged grains. The EDX/XRD analysis (Fig. 6) revealed that in the case of microwave sintering, there is an ongoing decarburization process. There can be two explanations of this process: first, carbon-free tungsten particles may be formed during the neck formation process and, as in case of (Fig. 4 (D1) – MWS), formation of liquid phase regions may be possible. Having said that, it should be clarified that tungsten carbide decomposes at temperatures higher than 2700 °C; therefore, the carbon-free tungsten areas that are formed during microwave sintering could be attributed to zones where the local temperature exceeded this limit. The other explanation is a difference in the C and W diffusivity in the WC system; another factor that may favor the decarburization process is the atmosphere used during sintering [48], to exclude this factor, nitrogen gas was used for sintering experiments [48,49].

As mentioned above for 1400 °C and applied high dwell times (F2) the most of the spheres observed were fully connected with an x/a ratio exceeding 0.3. Such structures can be explained by the external pressure applied during SPS experiments that naturally enhance both neck size and neck growth rate and may lead to formation of dense samples with further increases in processing time or temperature.

In the case of conventionally sintered particles (D3), the grain size in the neck zone and on the particles' surface is identical; clear boundaries between the grains are formed and surface smoothing (as for E3 – MWS) was not observed. The phase composition in the neck area and on the particles' surface was also defined as WC; no oxidized or carbon-free zones were observed in the case of conventional and spark-plasma sintering.

3.4. Numerical simulation of neck growth process

Although analysis of experimental data suggests surface, grain-boundary and volume diffusion to be the main sintering mechanisms responsible for neck growth during the initial stage of microwave, spark-plasma and conventional sintering of a given powder, it is important to estimate the diffusion coefficient responsible for neck growth. It is quite possible that higher temperatures exist at the contact zone as predicted [9,50] due to a relatively higher absorption of electromagnetic radiation at the grain boundaries/surfaces [51] in the case of microwave sintering, or due to known temperature gradient in case of the SPS [18,21]. Thus a partial melting may be possible as observed during microwave [32,52,53] and spark-plasma sintering of metals and ceramics [3,54].

In order to start with numerical simulation of the neck growth Eq. (1) was changed into

$$X = (X_*^n + B_z(t - t_*))^{1/n} \quad (3)$$

where X represents neck size at given time and temperature, the X_* be the neck size at t_*, where t_* is equal to 10 min. More detail explanation provided elsewhere [26,27].

Using Eq. (3), we may estimate the effective value of the diffusion coefficient by finding the correct value of rate constant B, which includes the diffusion coefficient. Values of δ, Ω and γ are taken from elsewhere [46] (Table 2), R is the gas constant, while a is equal to the particle radius, as reported earlier.

Values of diffusion coefficients obtained in this manner for spark-plasma sintering for temperatures of 900 and 1200 °C are 8.2×10^{-13} and 5.41×10^{-8} m^2 s^{-1} and presented in Fig. 7(a) and (b). Simulation of the neck growth process allows us to compute an effective diffusion coefficient for all processing temperatures, and the inverse slope in Fig. 8. Resulting activation energy of the

Table 2
Material constants for computer simulations.

Particle radii (μm)	Atomic volume (m^3)	Surface energy (J m^{-2})	Diffusion layer thickness (m)
62	2.59×10^{-29}	2.45	5×10^{-6}

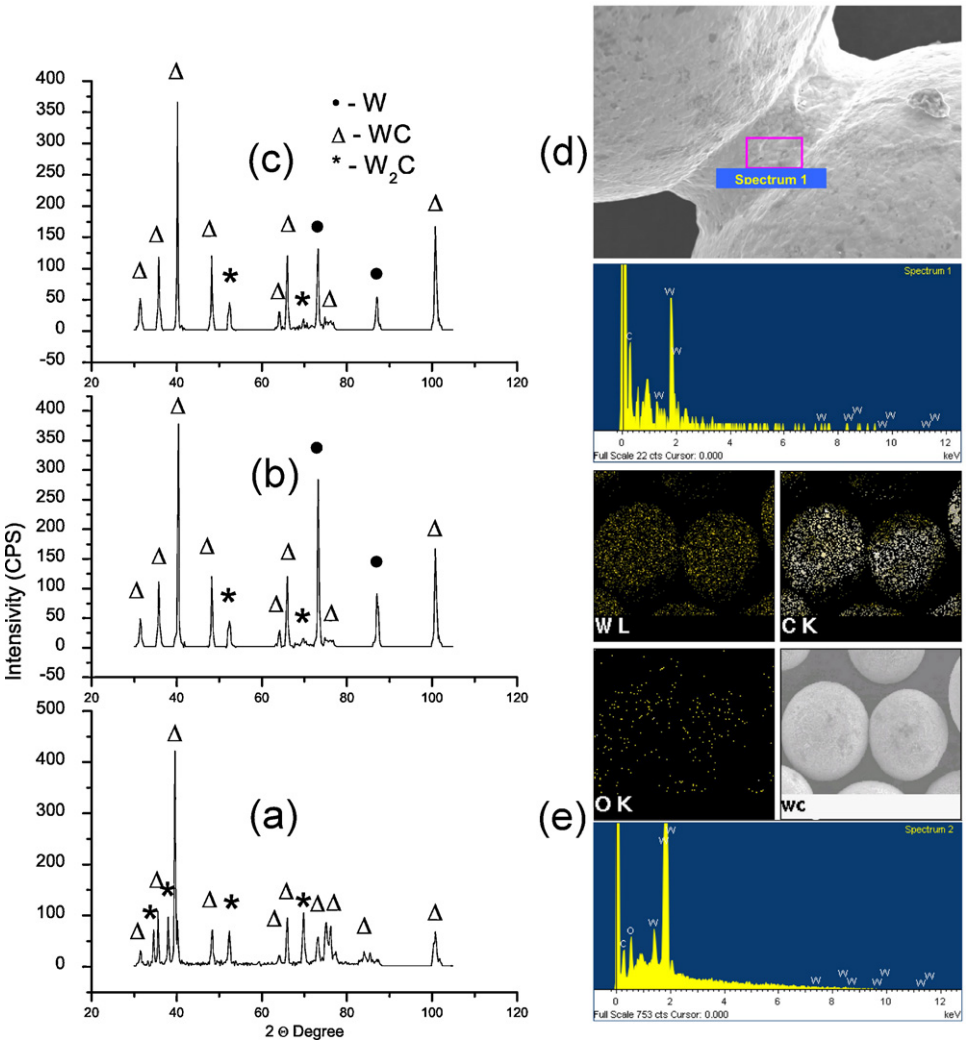

Fig. 6. Evidence of decarburization process during microwave sintering of WC powders at (b and d) 1200 and (c) 1400 °C for 30 min; (a) and (e) are the XRD and EDX for starting powder, respectively.

neck growth process is $52.5 \pm 2.9\,kJ\,mol^{-1}$. In recent study Nanda Kumar et al. [55] obtained activation energy of $45\,kJ\,mol^{-1}$ based on constant rate heating experiments on nanocrystalline WC powder. Studies by the Dorn method ($56\,kJ\,mol^{-1}$) were also performed and the anomalously low activation energy was explained as the combination of grain-boundary diffusion and the grain-growth process [55]. As for microwave sintering the diffusivities of 7.02×10^{-13} (Fig. 7(c)) and $3.41 \times 10^{-8}\,m^2\,s^{-1}$ were found at 900 and 1200 °C, respectively with an activation energy of. $69.2 \pm 3.1\,kJ\,mol^{-1}$ [27].

Surprisingly, diffusion coefficients obtained for SPS and MWS are at the same level; only at temperatures higher than 1200 °C, it is much higher in the case of SPS. Which is a quite interesting as far as SPS is generally considered as one of the fastest sintering methods [54,56,57]. In fact, in present investigation (Fig. 1) effect of external microwave field seems to be equal to the combined effect of electric current and external pressure. The latter seems to provide the additional driving force during initial stage sintering at higher temperatures (Fig. 7(b)), rather than at low-temperatures as accepted generally [54,57]. In both cases (MWS and SPS) diffusivities obtained strongly depend on the sintering temperature (Table 3) and are 8-fold higher than that observed by radio-tracer techniques [46,47,58–61].

Thus the comparison with the diffusion coefficient for conventional sintering becomes of great importance. The resulting effective diffusion coefficient for the temperature 1200 °C is $8.6 \times 10^{-16}\,m^2\,s^{-1}$ (Fig. 7(d)); there is a slight increase in diffusivity up to $5.6 \times 10^{-15}\,m^2\,s^{-1}$ with a further increase in temperature (1400 °C). The resulting values of activation energy $272.0\,kJ\,mol^{-1}$ and diffusivities calculated are in good agreement with data on diffusion in the W–C system by radio-tracer techniques [47,58–61].

3.5. Analysis of the sintering mechanisms

The values of apparent activation energies calculated for SPS and MWS are significantly lower than any data on diffusion in this system at a given temperature interval [53,57–61]. This fact, along with the value of diffusion coefficients may show, that for this case, mass transport was either supported by an additional driving force [9,62], or it is due to the local overheating.

It is unlikely that mechanisms of electromigration [22] or reduction of oxide surface [8] that where observed during neck growth kinetics during SPS of Cu and W, respectively, are active during SPS of WC. Therefore in case of SPS, a slight decline in the sintering rate exponent at higher processing temperatures (Table 3) (Fig. 9) might be an indication of an increase in the contribution of a pressure-applied mechanism (i.e., power-law creep) to the grain-boundary diffusion, as it is supported by the microstructures for

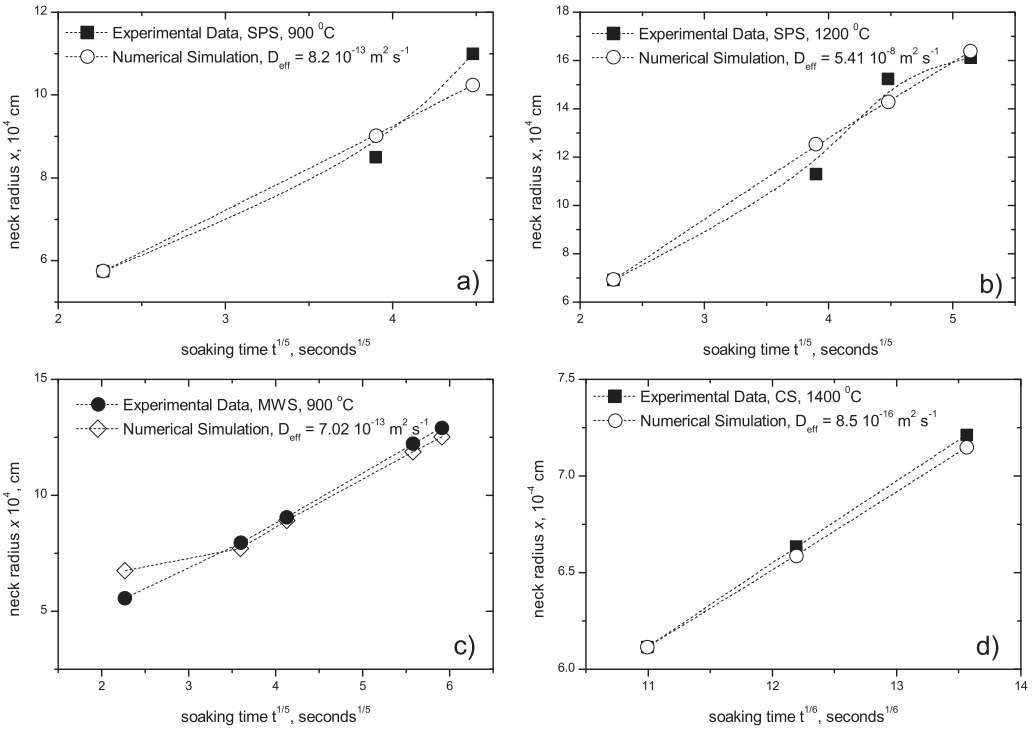

Fig. 7. Numerical simulation of neck growth process for (a) and (b) spark-plasma, (c) microwave, and (d) conventional sintering.

Table 3
Sintering experiments data.

Sintering method	Temperature (°C)	Sintering rate exponent, n	Effective diffusivity, D_{eff} ($m^2\ s^{-1}$)	Activation energy, Q_a ($kJ\ mol^{-1}$)
MWS	900–1000	5.05–5.2	7×10^{-13}	62
MWS	1200–1400	7.0–7.2	10^{-8}	50
SPS	900	5.04	8.2×10^{-13}	52
SPS	1200–1400	4.8	10^{-8} to 10^{-7}	52
CS	1200–1400	5.9–6.0	10^{-16} to 10^{-15}	272

applied high soaking times and predicted for the SPS processing of ceramics [63–65] and metals [17].

In case of MWS, the quick formation of liquid phase in the neck region is more likely explanation for the high diffusivities observed. It was previously shown for the case of MWS that at contact areas between the particles the value of the electrical field may be significantly higher than that generally in the volume of the resonant cavity [50,66]. Experimentally such mechanisms was observed during MWS of Ni powder [26] and was possible only due to a high gradient in the electromagnetic field [21] and creation of eddy currents on the particles' surface [32,53]. Like in the present study the n values of 5 was observed, that is similar for the initial stage during liquid-phase sintering for conventional sintering [67,68].

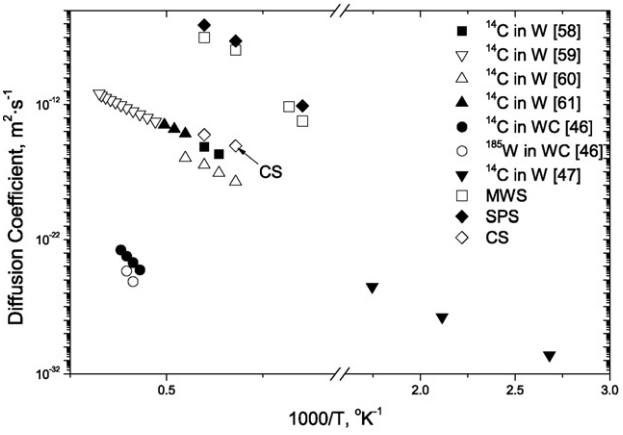

Fig. 8. Diffusion coefficients in the W–C system.

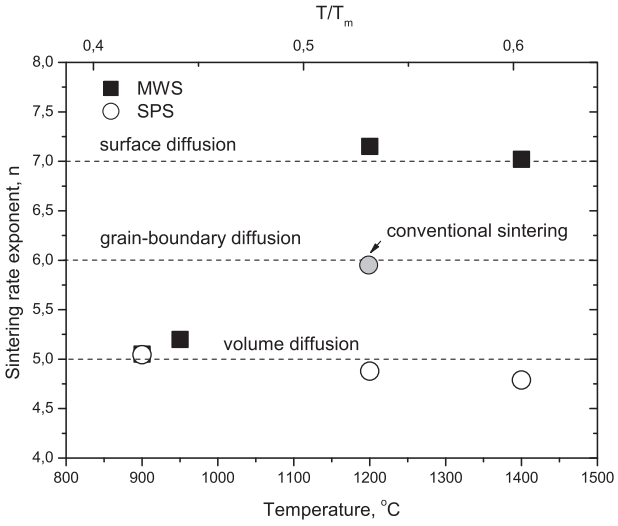

Fig. 9. Sintering rate exponent values resulting from the current investigation.

Nevertheless, though formation of a liquid phase during the initial stage of microwave sintering may be possible, as it is supported by higher values of diffusivities [26,69] and lower activation energies [27,53], the question of experimental evidences of liquid phase (similar to that in Fig. 4 (D3) – MWS) should be addressed in further work.

In the case of conventional sintering, the activation energy, neck growth exponent (Table 3), neck growth rate (Fig. 5) and the value of the diffusion coefficient suggest that grain-boundary diffusion was active as the predominant mechanism of mass transport during neck growth between WC particles. To complete initial stage of sintering $(x/a) \sim 0.3$ at temperatures of 1200/1400 °C dwell time of at least 725 h should be applied, that is at by 100-fold higher than that for SPS and MWS.

4. Conclusions

This study emphasizes the use of the neck growth kinetics approach to determine the main mass transport mechanisms during spark-plasma sintering, microwave and conventional sintering of spherically shaped tungsten carbide powder.

A detailed study of the neck growth mechanisms of tungsten carbide during the initial stage of sintering was carried out, and an analytical sphere-to-sphere model for the initial stage sintering of ceramics was successfully applied. The establishment of a sintering rate exponent (n) and of the apparent activation energy (E_a) values from sintering data coupled with SEM observations of sintered samples allowed some hypotheses on the sintering mechanisms of tungsten carbide, which are summarized below:

mass transport during SPS is substantially enhanced by applied stress and induction of eddy currents on the particle's surface and is governed by a combination of the mechanism of grain-boundary diffusion and power-law creep.
mass transport during microwave sintering is substantially enhanced by introduction of a small amount of a liquid phase and is governed by the mechanism of volume diffusion, which is followed by surface diffusion.

Low values of the apparent activation energy (E_a) for microwave and spark-plasma sintering (62 and 52 kJ mol^{-1}) have been obtained, and for conventional sintering, all data collected indicate grain-boundary diffusion as the main sintering mechanism (272 kJ mol^{-1}).

Numerical simulation of neck growth revealed high values of the diffusion coefficient for microwave and spark-plasma sintering, and for conventional sintering, the diffusion coefficients calculated are in good agreement with values for the diffusion of W and C in the W–C system.

Acknowledgements

The work was financially supported by STCU # 4259 which is gratefully acknowledged by D. Demirskyi and A. Ragulya. H. Borodianska acknowledges support from Nano-Ceramic Center of NIMS, Japan. The authors express their thanks to Prof. Clive A. Randall (PSU) and Prof. M.S. Kovalchenko (IPMS) for valuable suggestions and discussions. The authors also thank A.P. Zhurda from Paton EWI for preparing the WC spherical shaped particles.

References

[1] S. Grasso, Y. Sakka, G. Maizza, Sci. Technol. Adv. Mater. 10 (2009), 053001, 24 pp.
[2] R. Orru, R. Licheri, A.M. Locci, A. Cincotti, G. Cao, Mater. Sci. Eng. R 63 (2009) 127–287.
[3] R. Chaim, R. Marder-Jaeckel, J.Z. Shen, Mater. Sci. Eng. A 429 (2006) 74–78.
[4] H. Borodianska, T. Ludvinskaya, Y. Sakka, I. Uvarova, O. Vasylkiv, Scripta Mater. 61 (2009) 1020–1023.
[5] H. Borodianska, O. Vasylkiv, Y. Sakka, J. Nanosci. Nanotechnol. 8 (2008) 3077–3084.
[6] G. Suarez, H. Borodianska, Y. Sakka, E.F. Aglietti, O. Vasylkiv, J. Nanosci. Nanotechnol. 10 (2010) 6634–6640.
[7] R. Chaim, A. Shlayer, C. Estournes, J. Eur. Ceram. Soc. 29 (2009) 91–98.
[8] Z.A. Munir, D.V. Quach, M. Ohyanagi, J. Am. Ceram. Soc. 94 (2011) 1–19.
[9] R. Raj, M. Cologna, J.S.C. Francis, J. Am. Ceram. Soc. 94 (2011) 1941–1965.
[10] K.R. Anderson, J.R. Groza, M. Fendorf, C.J. Echer, Mater. Sci. Eng. A 270 (1999) 278–282.
[11] D.M. Hulbert, A. Anders, D.V. Dudina, J. Andersson, D. Jiang, C. Unuvar, U. Anselmi-Tamburini, E.J. Lavernia, A.K. Mukherjee, J. Appl. Phys. 104 (2008), 033305, 7 pp.
[12] M. Hulbert, A. Anders, J. Anderson, E.J. Lavernia, A.K. Mukherjee, Scripta Mater. 60 (2009) 835–838.
[13] J.E. Garay, U. Anselmi-Tamburini, Z.A. Munir, Acta Mater. 51 (2003) 4487–4495.
[14] N. Bertolino, J. Garay, U. Anselmi-Tamburini, Z.A. Munir, Philos. Mag. B 82 (2002) 969–985.
[15] L.A. Stanciu, V.Y. Kodash, J.R. Groza, Metall. Mater. Trans. A 32A (2001) 2633–2638.
[16] E.A. Olevsky, S. Kandukuri, L. Froyen, J. Appl. Phys. 102 (2007), 114913, 12 pp.
[17] E.A. Olevsky, L. Froyen, J. Am. Ceram. Soc. 92 (2009) S122–S132.
[18] M. Cologna, B.B. Rashkova, R. Raj, J. Am. Ceram. Soc. 93 (2010) 3556–3559.
[19] K. Vanmeensel, A. Laptev, J. Hennicke, J. Vleugels, O. Van der Biest, Acta Mater. 53 (2005) 4379–4388.
[20] D. Tiwari, B. Basu, K. Biswas, Ceram. Int. 35 (2009) 699–709.
[21] D. Demirskyi, H. Borodianska, S. Grasso, Y. Sakka, O. Vasylkiv, Scripta Mater. 65 (2011) 683–686.
[22] J.M. Frei, U. Anselmi-Tamburini, Z.A. Munir, J. Appl. Phys. 101 (2007) 1–8, 114914.
[23] M. Cologna, R. Raj, J. Am. Ceram. Soc. 94 (2011) 391–395.
[24] D. Demirskyi, D. Agrawal, A. Ragulya, Scripta Mater. 86 (2010) 552–555.
[25] D. Demirskyi, A. Ragulya, Powder Metall. Met. Ceram. 49 (2010) 147–152.
[26] D. Demirskyi, D. Agrawal, A. Ragulya, J. Alloys Compd. 509 (2011) 1790–1795.
[27] D. Demirskyi, A. Ragulya, D. Agrawal, Ceram. Int. 37 (2011) 505–512.
[28] D. Agrawal, Curr. Opin. Mater. Sci. 3 (1998) 480–486.
[29] G.C. Kuczynski, Metall. Trans. AIME 185 (1949) 169–178.
[30] W.D. Kingery, M. Berg, J. Appl. Phys. 26 (1955) 1205–1212.
[31] G. Maizza, S. Grasso, Y. Sakka, T. Noda, O. Ohashi, Sci. Technol. Adv. Mater. 8 (2007) 644–654.
[32] D. Demirskyi, D. Agrawal, A. Ragulya, Mater. Sci. Eng. A 527 (2010) 2142–2145.
[33] L.S.-J. Kang Sintering, Densification Grain Growth and Microstructure, Elsevier, Amsterdam, 2005.
[34] D. Lynn Johnson, J. Appl. Phys. 40 (1969) 192–200.
[35] N.M. Rahaman, Ceramic Processing and Sintering, Second ed., CRC Press, New York, 2003.
[36] R.M. German, S.J. Park, Mathematical Relations in Particulate Materials Processing: Ceramics, Powder Metals, Cermets, Carbides, Hard Materials and Minerals, Wiley Interscience, New York, 2008.
[37] T.L. Wilson, P.G. Shewmon, Trans. AIME 236 (1966) 48–58.
[38] F.B. Swinkels, M.F. Ashby, Acta Metall. 29 (1981) 259–281.
[39] D. Lynn Johnson, I.B. Cutler, Acta Metall. 12 (1964) 1173–1179.
[40] D. Lynn Johnson, I.B. Cutler, J. Am. Ceram. Soc. 46 (1963) 541–545.
[41] R. Chaim, M. Margulis, Mater. Sci. Eng. A 407 (2005) 180–187.
[42] R.L. Coble, in: G.C. Kuczynski (Ed.), Sintering and Related Phenomena, Plenum Press, New York, 1973, pp. 177–189.
[43] A.V. Ragulya, V.V. Skorokhod, Consolidated Nanostructured Materials, Naukova dumka, Kiev, 2007 [in Russian].
[44] F. Thumler, W. Thomma, Metall. Rev. 12 (1967) 69–108.
[45] M.F. Ashby, Acta Metall. 22 (1974) 275–289.
[46] R.A. Andrievky, I.I. Spivak, Strenth of High Melting Point Compounds. A Companion, Metallurgy, Moscow, 1983 [in Russian].
[47] A.D. LeClaire, G. Neumann, in: H. Mehrer (Ed.), Diffusion in Solid Metals and Alloys (Ref. 68S1), Springer-Verlag, Berlin/Heidelberg, 1990, p. 480.
[48] P. Bague, J.P. Morizot, G. Desgardin, J. Phys. D: Appl. Phys. 27 (1994) 402–405.
[49] P. Schwarzkopf, R. Kieffer, Cemented Carbides, MacMillan, New York, 1986.
[50] A. Birnboim, J.P. Calame, Y. Carmel, J. Appl. Phys. 85 (1999) 478–482.
[51] E. Breval, J.P. Cheng, D.K. Agrawal, P. Gigl, M. Dennis, R. Roy, A.J. Papworth, Mater. Sci. Eng. A 391 (2005) 285–295.
[52] G. Veltl, F. Petzold, P.A. Pueschner, Powder Metallurgy 2004 World Congress.
[53] D. Demirskyi, D. Agrawal, A. Ragulya, Mater. Lett. 64 (2010) 1433–1436.
[54] V. Mamedov, Powder Metall. 45 (2002) 322–328.
[55] A.K. Nanda Kumar, M. Watabe, K. Kurokawa, Ceram. Int. 37 (2011) 2643–2654.
[56] J.R. Groza, A. Zavaliangos, Mater. Sci. Eng. A 287 (2000) 171–177.
[57] Z.A. Munir, U. Andelmi-Tamburini, M. Ohyanagi, J. Mater. Sci. 41 (2006) 763–777.
[58] L.N. Aleksandrov, V.Y. Shchelkonogov, Sov. Powder Metall. Met. Ceram. 3 (4) (1964) 288–291.
[59] A.D. LeClaire, G. Neumann, in: H. Mehrer (Ed.), Diffusion in Solid Metals and Alloys (Ref. 65K), Springer-Verlag, Berlin/Heidelberg, 1990, p. 480.
[60] A.D. LeClaire, G. Neumann, in: H. Mehrer (Ed.), Diffusion in Solid Metals and Alloys (Ref. 66N1), Springer-Verlag, Berlin/Heidelberg, 1990, p. 480.
[61] A. Shepela, J. Less Common Met. 26 (1972) 33–43.
[62] Y.V. Bykov, S.V. Egorov, A.G. Eremeev, K.I. Rybakov, V.E. Semenov, A.A. Sorokin, S.A. Gusev, J. Mater. Sci. 26 (2011) 131–136.

[63] G. Bernard-Granger, C. Guizard, Acta Mater. 55 (2007) 3493–3504.
[64] J. Langer, M.J. Hoffmann, O. Guillon, Acta Mater. 57 (2009) 5454–5465.
[65] O. Guillon, J. Langer, J. Mater. Sci. 45 (2010) 5191–5195.
[66] A. Birnboim, T. Olorunyolemi, Y. Carmel, J. Am. Ceram. Soc. 84 (2001) 1315–1320.
[67] W.D. Kingery, J. Appl. Phys. 30 (1959) 301–306.
[68] T.H. Courtney, Metall. Trans. A 8A (1977) 671–677.
[69] D. Demirskyi, D. Agrawal, A. Ragulya, Scripta Mater. 66 (2012) 323–326.